Transport spectroscopy of disordered graphene quantum dots etched into a single graphene flake

Dominikus Kölbl and Dominik M. Zumbühl*

Department of Physics, University of Basel, Klingelbergstrasse 82, CH-4056 Basel, Switzerland

(Dated: August 1, 2013)

We present transport measurements on quantum dots of sizes 45, 60 and 80 nm etched with an Ar/O$_2$-plasma into a single graphene sheet, allowing a size comparison avoiding effects from different graphene flakes. The transport gaps and addition energies increase with decreasing dot size, as expected, and display a strong correlation, suggesting the same physical origin for both, i.e. disorder-induced localization in presence of a small confinement gap. Gate capacitance measurements indicate that the dot charges are located in the narrow device region as intended. A dominant role of disorder is further substantiated by the gate dependence and the magnetic field behavior, allowing only approximate identification of the electron-hole crossover and spin filling sequences. Finally, we extract a g-factor consistent with $g = 2$ within the error bars.

Spins in condensed matter systems have become an important field of research motivated by spintronics and quantum information and the underlying fundamental physics. Graphene has several exceptional properties[1] and is an exciting material promising long spin relaxation and coherence times as a result of weak spin-orbit interaction and weak hyperfine effects due to the predominant natural abundance of the nuclear-spin free ^{12}C[2,3]. Recent progress taking micron-scale 2D systems[4,5] to nano-scale ribbons and quantum dots has opened the door to study the physics of confined charges and spins in graphene[6–11], paving the way towards nano-device applications. Challenges include overcoming the gapless nature of graphene[6–8], defining tunnel barriers[9], and achieving controlled tunability of devices[12].

Despite these significant advances, most experiments in graphene nano-devices are currently dominated by disorder, often masking the intrinsic (graphene) physics. Disorder is thought to arise from surface, substrate and edge imperfections as well as intrinsic graphene defects. Investigating and suppressing disorder is therefore crucial for further progress. Further, when studying graphene nano-devices, it is important to change the relevant parameters such as dot size or ribbon width without significantly or qualitatively changing disorder. Here, we report electronic transport spectroscopy of quantum dots of three different sizes fabricated on the same graphene sheet with essentially identical disorder broadening of the Landau levels across the entire graphene flake.

The devices are approximately square-shaped graphene quantum dots with designed widths $w = 45$, 60, and 80 nm placed on the same graphene sheet exfoliated from HOPG onto a Si wafer[14] with a back-gate separated by a 294 nm thick oxide[15]. Ti/Au (5/40 nm) contacts are defined via standard e-beam lithography (EBL). Dots with slightly narrower junctions to the graphene reservoirs are etched with an Ar/O$_2$ plasma using a PMMA-mask predefined in a second EBL step. The insets in Figure 1a-c show AFM images of each dot. Graphene regions separated from the dots by ~ 20 nm wide etched trenches are also contacted and used for side gating the dots individually with side-gate voltage V_{SG}. The overall charge
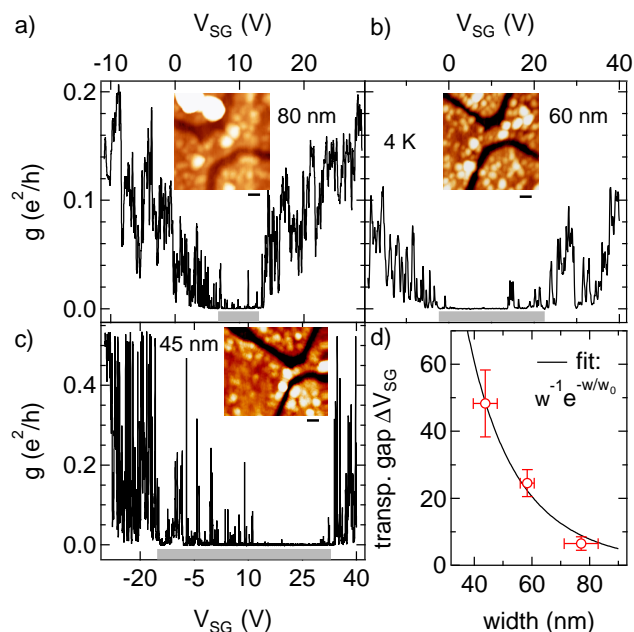

FIG. 1: Transport gaps at 4K. (a)-(c) Zero dc-bias differential conductance g as a function of side gate voltage V_{SG} for each dot as labeled. The grey bars indicate the transport gap ΔV_{SG}, defined as the V_{SG} range where the valley conductances remain smaller than 10^{-4} e^2/h. The insets show AFM-images (all scale bars 50 nm). White speckles presumably are PMMA or other residues. (d) Transport gap ΔV_{SG} determined from (a)-(c) (open circles) as a function of dot size. The solid curve is a fit to Ref.[13], see text.

density can be tuned with back-gate voltage V_{BG}.

Two-terminal measurements in the quantum Hall regime[16] using bulk regions of the flake showed it to be single-layer graphene. We extract a field-effect mobility of about 3'000 cm^2/Vs at a density of 2×10^{11} cm^{-2} before removal of PMMA. This mobility is a lower bound as the PMMA was removed prior to the measurements presented below. High-field Landau level broadening in the four graphene regions surrounding the three quantum dots distributed across the ~ 20 μm long graphene sheet was essentially identical in each region, indicating ho-

mogeneous disorder across the entire graphene flake and therefore for all three dots, allowing a size-comparison of transport properties without significantly changing disorder. The back-gate voltage $V_{BG} = 0$ except where stated otherwise. Measurements are performed in a dilution refrigerator unit at $T = 4\,K$ and $T \sim 100\,mK$ (electron temperature). Conductance across the graphene nano ribbons (GNRs) is probed with a standard lock-in technique using a small ac modulation on top of a variable dc-bias.

First, we investigate the transport gap as a function of side-gate voltage V_{SG} for each dot, shown in Figure 1a-c at 4K. Around the charge neutrality point (CNP) located within a few volts from zero gate voltage similar for all dots, we find a strongly suppressed conductance with sharp characteristic Coulomb blockade (CB) peaks over a wide range of gate voltages and strong conductance fluctuations at elevated densities, both typical for GNR devices measured at low temperatures[6,8-10]. We introduce ΔV_{SG} as the V_{SG}-range where the CB valley conductances remain smaller than $10^{-4}\,e^2/h$, as indicated by the grey bars in Figure 1a-c. The resulting transport gap, shown in Figure 1d, is strongly size dependent, giving larger gaps for the smaller devices, as expected[6,17,18].

Several theories predict the formation of a confinement gap E_g in graphene, including tight-binding[19], ab-initio[20], Anderson localization[21], and many-body theory[13], all giving similar results. The latter suggests a width w dependence given by $E_g \sim w^{-1}e^{-(w/w_0)}$ (with decay length w_0), which is widely used to analyze experimental results and also fits our data $\Delta V_{SG}(w)$ quite well using $w_0 = 29.4 \pm 4.2\,nm$ (see Fig.1(d)). However, converting ΔV_{SG} to energy ($\delta E = \alpha_{SG} \cdot \Delta V_{SG}$) using an average lever arm $\alpha_{SG} = 0.117 \pm 0.049$ eV/V extracted from CB diamonds (see below, Fig.2(c)) results in an absolute energy scale of several eV, far exceeding predictions for a simple confinement induced band gap by about two orders of magnitude. Therefore, the transport gap ΔV_{SG} most likely is not due to geometric confinement only. Further, the appearance of numerous CB peaks (rather than a large region of very low conductance) and conductance fluctuations surrounding the transport gap indicate the strong influence of disorder. A large transport gap could then result from disorder localization and Coulomb blockade in presence of a much smaller confinement gap necessary to inhibit Klein tunneling[22].

Possible sources of this disorder include graphene defects and edge disorder, trapped charges nearby, partially due to adsorbates and PMMA residues which are clearly visible in AFM images throughout the devices (see Figure 1, insets), as well as other substrate and surface disorder. However, since all dots are fabricated on the same graphene sheet showing nearly identical Landau level broadening in all regions across its length, we expect this disorder to be of similar quality for the three dots. We note that the importance of a fabrication induced edge roughness of the order of a few nm should increase from the 80 nm to the 45 nm device, where it is reaching 10%
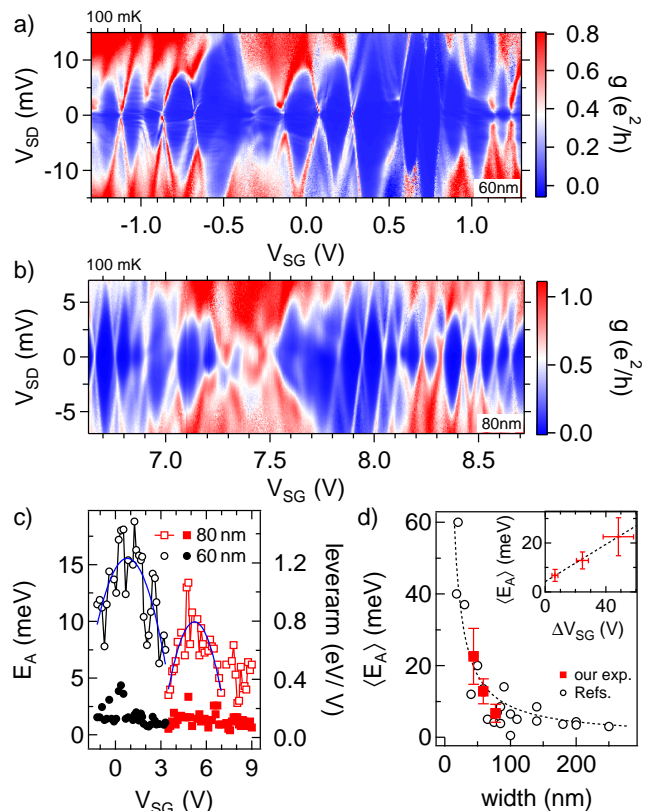

FIG. 2: Coulomb diamonds (a),(b) Differential conductance (color scale) as a function of source-drain voltage V_{SD} and side-gate voltage V_{SG} at $T \sim 100$ mK of the 60 and 80 nm dots, as labeled. (c) Addition energies (left axis, open symbols) and corresponding V_{SG} lever arms (right axis, filled symbols) from Coulomb diamonds as in (a) and (b) but with extended V_{SG} range. Blue curves (parabolas) are shown as a guide to the eye, indicating a peak in E_A at the CNP for both dots, also confirmed by $B_\perp$ data, see text. (d) Size-dependence of the average addition energy $\langle E_A \rangle$ (squares). Error bars denote standard deviation. Circles are from Refs.[8,9,12,17,24-28]. The dashed curve is an ϵ/w fit with $\epsilon = 870 \pm 70$ meV nm, see text. The inset shows $\langle E_A \rangle$ vs. ΔV_{SG} with a line fit (dashed black) indicating a strong correlation.

of the device width[21,23].

Clear Coulomb diamonds are seen in finite bias measurements for all three dots, shown in Figure 2a,b for the larger dots at 100 mK, indicating the formation of a tunnel coupled quantum dot in the transport gap region. We find signatures of excited states in sequential tunneling (typically at $\sim$meV energies), but also cotunneling features. We extract the addition energies E_A and V_{SG} lever arms from similar data extending over a larger V_{SG}-range for the two larger dots, shown in Figure 2c. Both dots show similar lever arms, as expected due to similar geometry, roughly independent of V_{SG}. The addition energies are larger in the smaller dot, on average, as expected. Further, a maximum in E_A as a function of V_{SG} – indicated by the blue curves – is seen close to the bulk CNP, roughly marking the electron-to-hole crossover. However,

we cannot identify the zero-occupation diamond and the absolute charge-number in these dots, though the expected confinement-induced band gap[20] is comparable to the observed addition energies.

The size dependence of the average addition energy $\langle E_A \rangle$ obtained from Coulomb diamond measurements over a large gate voltage range is shown in Figure 2d (red squares), in good agreement with previous reports of similar size devices (black circles)[8,9,12,17,24–27,29]. A fit to the single dot theory $\langle E_A \rangle = \epsilon/w$[13] gives decent agreement (see dashed curve), resulting in $\epsilon = 870 \pm 70 \,\mathrm{meV\,nm}$, comparable with other experiments[6,18]. Interestingly, for the present three dots, we find a clear correlation between the average addition energy $\langle E_A \rangle$ and the transport gap size ΔV_{SG} (see inset Figure 2d), suggesting the same physical origin for both energy scales.

Further, we can estimate the effective dot area via the back-gate capacitance taken from diamonds and using a simple parallel plate capacitor model[30]. This simple model should give a good estimate of the area for the larger devices, where the etched trenches defining the dots in the otherwise continuous graphene layer are narrow compared to the device diameter. We note that the simple plate capacitor model used here for the back-gate does not apply to the total capacitance, which is significantly larger than the back-gate capacitance. The extracted areas agree well (within the error bars of $\sim 15\,\%$) with the actual dot sizes (from AFM scans) for the two larger devices, suggesting that the electrons are indeed located in the lithographically intended region of the GNR. Overall, the above results seem to indicate predominant formation of single quantum dots in these devices.

However, we also find a number of overlapping diamonds or diamonds that do not close at low bias, indicating formation of double or multiple dots[31] in a repeatable way (during the same cool down) as a function of gate voltage. This is further substantiated by V_{SG} and V_{BG} scans shown in Figure 3a,b. Regions in gate space of parallel lines with a fixed slope (given by the relative side- and back-gate leverarms) characteristic for a single dot are alternating with non-parallel, honey-comb like features[7,25,32] (again repeatable in gate voltage), indicating double or multiple-dot formation[33], presumably as a result of the pronounced disorder potential. As gate voltage is changed monotonously, the dot appears to sporadically rearrange its geometry, deforming between a simple, single dot and more complicated configurations.

We now turn to perpendicular magnetic field $B_\perp$ measurements, shown in Figure 3c-e for all three dots at $V_{SD} = 0$ and $T = 100\,\mathrm{mK}$. Besides a strong variation of the peak conductance, the peak positions of the 80 nm-device bend towards $V_{SG} \sim 5\,\mathrm{V}$ for large $B_\perp$, as expected for the $0th$ graphene Landau level at the CNP[26,34,35]. Therefore, we can extract the CNP in this device to be located around 5 V, consistent with the highest value of E_A found for $V_{SG} = 4.8\,\mathrm{V}$ (Figure 2c). Similarly, for the 60 nm device, the electron-hole crossover is found around $V_{SG} \sim 1\,\mathrm{V}$, again consistent with the previously deter-
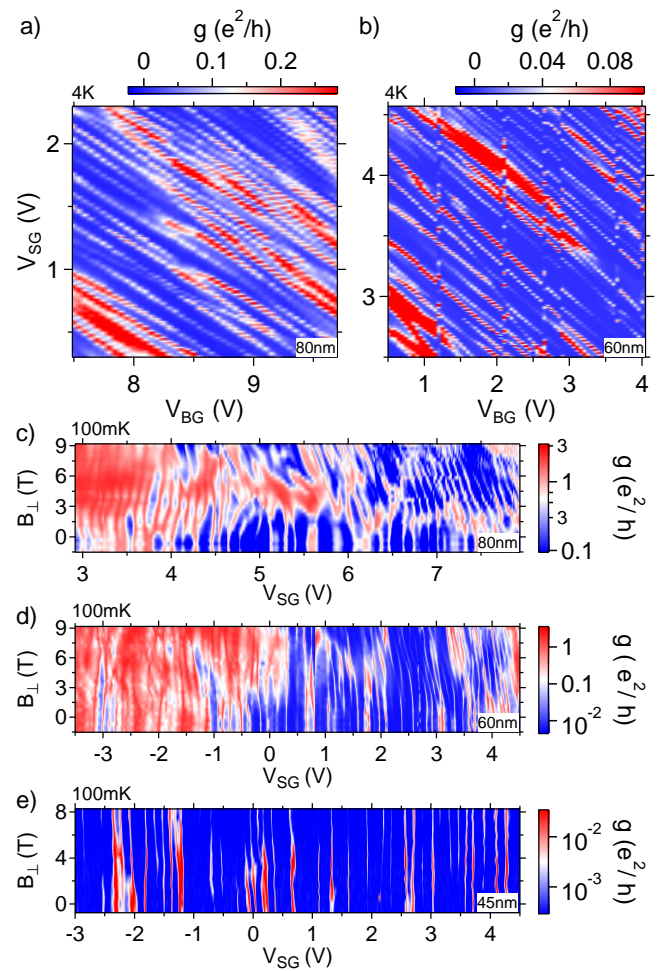

FIG. 3: Gate-gate sweeps and $B_\perp$ peak motion: (a),(b) Differential conductance showing CB peaks as a function of V_{SG} and V_{BG} at 4 K. Parallel lines indicating single dot behavior alternate with bending and merging features that can arise from multiple-dot formation (repeatable). (c)-(e) CB peak evolution in a perpendicular field $B_\perp$ of the 80, 60 and 45 nm dots at 100 mK. At large $B_\perp$, peaks bend towards the graphene zero Landau-level around the electron-hole transition ($V_{SG} \sim 5\,\mathrm{V}$ for 80 nm dot, and $V_{SG} \sim 1\,\mathrm{V}$ for 60 nm dot), more clearly visible for the larger dots, see text.

mined maximal E_A at $V_{SG} = 1.25\,\mathrm{V}$ (Figure 2c), though for this devices the $B_\perp$ bending of the peaks is weaker. Therefore, the CNPs in both dots are separated by only a few Volts, both close to zero. Landau level bending becomes visible at high fields when the magnetic length $l_B = \sqrt{\hbar/eB}$ is much smaller than the device size w[34,35], making the effect weakest in the smallest dot (Figure 3e).

Beyond Landau levels, paired peak motion due to consecutive filling of the same orbital with opposite spins (spin pairs) can also be observed in the $B_\perp$ dependence. Periods of four were not identifiable, suggesting a broken valley degeneracy in these dots. Spin pairs are most clearly visible for the largest device (where the $B_\perp$ effect is most pronounced), where some pairs particularly at high electron/hole densities away from the CNP exhibit
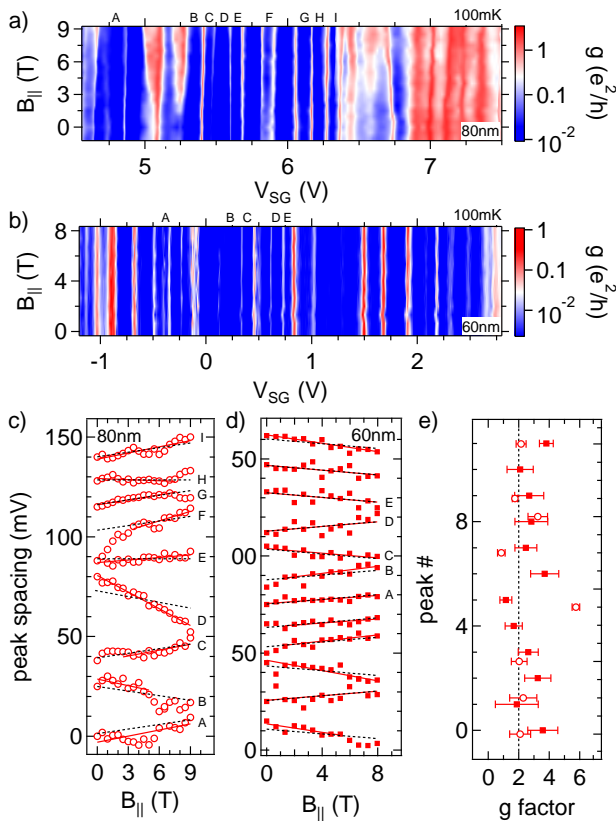
FIG. 4: $B_\parallel$ peak motion and g-factors: (a),(b) Differential conductance as a function of $B_\parallel$ and V_{SG} for the larger dots at 100 mK. (c),(d) Selection of CB peak spacings which are approximately linear in $B_\parallel$, offset for clarity, see text. Solid red lines are best linear fits. The extent of each line is the fit range used. For comparison, the $\pm g\mu_B$ and zero slopes are also shown (dashed black lines). (e) Summary of g-factors from (c) and (d) (excluding zero-slope data), with open circles for 80 nm dot and solid squares for 60 nm dot. Vertical positions are chosen to align with data in (c) and (d). Error bars are standard deviations from linear fits.

reproducible parallel evolution over a significant range in $B_\perp$, see e.g. Figure 3c, 3 V $< V_{SG} <$ 4.5 V. However, the low-density region around the CNP which is more strongly affected by disorder[35] appears more complicated and clear pairs could not be found, similar to the smaller dots, which are also more weakly coupled to the reservoirs. These efforts are further hampered by disorder driven dot rearrangements (single to double dot transitions as a function of V_{SG}) as described before and sporadic switching in gate voltage observed in these devices.

The evolution of the CB peak spacing in an in-plane magnetic field $B_\parallel$ can in principle reflect the spin filling sequence[36]. In graphene quantum dots, spin-orbit coupling can be assumed to be very weak and the Landé g-factor $g \sim 2$. For dot-diameters $d < 100$ nm, the orbital level spacing $\Delta > 2$ meV remains larger then the Zeeman splitting $E_Z = g\mu_B B$ (with Bohr magneton μ_B) for $B_\parallel \leq 10$ T. In this case, and if electron-electron interactions are negligible, one might expect a simple alter-

nating Pauli spin sequence giving peak spacings which increase or decrease with slope $g\mu_B$. $B_\parallel$-independent peak spacings (slope zero), however, would be absent in this simple picture, since these indicate a filling of two subsequent identical spins induced by interactions[36], resulting in total spin $S > 1/2$.

Figure 4a,b shows the CB peak positions of the 80 nm and 60 nm devices at 100 mK as a function of $B_\parallel$ (separate cool down) over a range of V_{SG} including the electron-hole transitions. We fit Gaussians to the CB peaks to obtain the peak positions and evaluate the peak spacing as a function of $B_\parallel$. While some peak spacings show the expected slopes (zero or $\pm g\mu_B$), others exhibit more complicated, nonlinear $B_\parallel$ dependence. This could be due to disorder driven dot-rearrangements as a function of V_{SG} as mentioned above, a slight $B_\parallel$ misalignment with a resulting $B_\perp$ component of $B_\parallel$ (a few degrees here) or other orbital coupling of $B_\parallel$, e.g. by threading flux through the graphene surface ripples[37].

In an attempt to avoid these $B_\parallel$ complications, we select peaks spacings approximately linear over a sufficiently large range of $B_\parallel$ without rejecting any slope, plotted in Figure 4c,d (offset for clarity), also labeled A-I and α-ϵ above their corresponding peaks in Figure 4a,b. We extract the slopes with best fits (solid red lines) and also indicate the closest standard slope (dashed black lines, slopes 0, $\pm g\mu_B$) for comparison, using the average lever arms previously measured from Coulomb diamonds of each dot. The resulting g-factors are summarized in Figure 4e for both dots. While in several cases, good agreement with the expected $g \sim 2$ is found (see e.g. A,B,C,G,I), we also notice horizontal, $B_\parallel$ independent peak spacings indicating non-trivial spin filling (e.g. H). Further, slopes strongly deviating from $g = 2$ are also seen, which is not surprising considering the $B_\parallel$ issues mentioned before. Nevertheless, averaging over the data in Figure 4e from both dots, we obtain $g = 2.7 \pm 1.1$ (excluding the obvious near-zero point H), consistent with $g = 2$ as expected and in line with other experiments[11,38,39].

In summary, we have presented transport spectroscopy of graphene quantum dots on the same graphene flake with nearly identical disorder broadening. This allows a size comparison without changing disorder, displaying the expected size dependence of transport gap and addition energy as well as clear correlation between both, suggesting disorder induced localization in presence of a confinement gap as the physical origin for both effects. Gate capacitance measurements indicate that the dot charges are located in the narrow device region as expected. Even though the electron-hole transitions could not be precisely located ($\pm$ few electrons) and the spin filling sequences were not fully tractable, both ultimately due to disorder, the average g-factor is consistent with $g = 2$, though with significant error bar.

Overall, the combined data clearly draw a consistent picture of pronounced disorder effects which are masking the interesting low-density, few electron regime in

these graphene devices. For future nano-graphene experiments, it will therefore be very important to investigate and suppress disorder, e.g. by removal of substrate[40] and adsorbate disorder, by a high degree of control over the graphene edges[29,41,42] and elimination of any residual intrinsic graphene defects.

[*] Electronic address: dominik.zumbuhl@unibas.ch

[1] A. H. Castro Neto, F. Guinea, N. M. R. Peres, K. S. Novoselov, and A. K. Geim, Rev. Mod. Phys. **81**, 109 (2009).

[2] J. Fischer, B. Trauzettel, and D. Loss, Phys. Rev. B **80**, 155401 (2009).

[3] B. Trauzettel, D. V. Bulaev, D. Loss, and G. Burkard, Nat. Phys. **3**, 192 (2007).

[4] K. S. Novoselov, A. K. Geim, S. V. Morozov, D. Jiang, M. I. Katsnelson, I. V. Grigorieva, S. V. Dubonos, and A. A. Firsov, Nature **438**, 197 (2005).

[5] Y. Zhang, Y.-W. Tan, H. L. Stormer, and P. Kim, Nature **438**, 201 (2005).

[6] M. Y. Han, B. Özyilmaz, Y. Zhang, and P. Kim, Phys. Rev. Lett. **98**, 206805 (2007).

[7] K. Todd, H. Chou, S. Amasha, and D. Goldhaber-Gordon, Nano Lett. **9**, 416 (2009).

[8] L. A. Ponomarenko, F. Schedin, M. I. Katsnelson, R. Yang, E. W. Hill, K. S. Novoselov, and A. K. Geim, Science **320**, 356 (2008).

[9] X. Liu, J. B. Oostinga, A. F. Morpurgo, and L. M. K. Vandersypen, Phys. Rev. B **80**, 121407 (2009).

[10] C. Stampfer, E. Schurtenberger, F. Molitor, J. Güttinger, T. Ihn, and K. Ensslin, Nano Lett. **8**, 2378 (2008).

[11] J. Güttinger, T. Frey, C. Stampfer, T. Ihn, and K. Ensslin, Phys. Rev. Lett. **105**, 116801 (2010).

[12] C. Stampfer, J. Güttinger, F. Molitor, D. Graf, T. Ihn, and K. Ensslin, Appl. Phys. Lett. **92**, 012102 (2008).

[13] F. Sols, F. Guinea, and A. H. Castro Neto, Phys. Rev. Lett. **99**, 166803 (2007).

[14] K. S. Novoselov, A. Geim, S. V. Morozov, D. Jiang, Y. Zhang, S. Dubonos, I. Grigorieva, and A. A. Firsov, Science **306**, 5696 (2004).

[15] P. Blake, E. W. Hill, A. H. Castro Neto, K. S. Novoselov, D. Jiang, R. Yang, T. J. Booth, and A. K. Geim, Appl. Phys. Lett. **91**, 063124 (2007).

[16] J. R. Williams, D. A. Abanin, L. Dicarlo, L. S. Levitov, and C. M. Marcus, Phys. Rev. B **80**, 045408 (2009).

[17] F. Molitor, A. Jacobsen, C. Stampfer, J. Güttinger, T. Ihn, and K. Ensslin, Phys. Rev. B **79**, 075426 (2009).

[18] F. Molitor, C. Stampfer, J. Güttinger, A. Jacobsen, T. Ihn, and K. Ensslin, Semicond. Sci. Technol. **25**, 034002 (2010).

[19] K. Nakada, M. Fujita, G. Dresselhaus, and M. S. Dresselhaus, Phys. Rev. B **54**, 17954 (1996).

[20] Y. W. Son, M. L. Cohen, and S. G. Louie, Phys. Rev. Lett. **97**, 216803 (2006).

[21] M. Evaldsson, I. Zozoulenko, H. Xu, and T. Heinzel, Phys. Rev. B **78**, 161407 (2008).

[22] M. I. Katsnelson, K. S. Novoselov, and A. K. Geim, Nat. Phys. **2**, 620 (2006).

[23] E. R. Mucciolo, A. H. Castro Neto, and C. H. Lewenkopf, Phys. Rev. B **79**, 075407 (2009).

[24] S. Schnez, F. Molitor, C. Stampfer, J. Güttinger, I. Shurobalko, T. Ihn, and K. Ensslin, Appl. Phys. Lett. **94**, 012107 (2009).

[25] C. Stampfer, J. Güttinger, S. Hellmüller, F. Molitor, K. Ensslin, and T. Ihn, Phys. Rev. Lett. **102**, 056403 (2009).

[26] J. Güttinger, C. Stampfer, F. Libisch, T. Frey, J. Burgdörfer, T. Ihn, and K. Ensslin, Phys. Rev. Lett. **103**, 046810 (2009).

[27] S. Neubeck, L. A. Ponomarenko, F. Freitag, A. J. M. Giesbers, U. Zeitler, S. V. Morozov, P. Blake, A. K. Geim, and K. S. Novoselov, Small **6**, 1469 (2010).

[28] L.-J. Wang, G. Cao, T. Tu, H.-O. Li, C. Zhou, X.-J. Hao, G.-C. Guo, and G.-P. Guo, Chin. Phys. Lett. **28**, 067301 (2011).

[29] X. Wang, Y. Ouyang, L. Jiao, H. Wang, L. Xie, J. Wu, J. Guo, and H. Dai, Nature Nanotech. **6**, 563 (2011).

[30] We extract the backgate capacitance using $C_{BG} = e/\delta V_{BG} = e/(\alpha_{rel} \cdot \delta V_{SG})$ and compare it to a parallel plate capacitor with $C_{pp} = \epsilon\epsilon_0 \cdot A/d$ where $\delta V_{BG}, \delta V_{SG}$ are the average voltages for adding one electron with the respective gate, α_{rel} is the relative side/back gate lever arm (from Fig. 3a,b), $\epsilon = 3.9$ for SiO_2 with thickness $d = 294\,\mathrm{nm}$, ϵ_0 is the vacuum permittivity, and A is the dot area. We obtain $A = 87^2\,\mathrm{nm}^2$ and $A = 59^2\,\mathrm{nm}^2$, compared to AFM scan dimensions of $A = 80 \times 90\,\mathrm{nm}^2$ and $A = 60 \times 67\,\mathrm{nm}^2$, respectively, giving good agreement within the error bars of $\sim 15\%$.

[31] S. Dröscher, H. Knowles, Y. Meir, K. Ensslin, and T. Ihn, Phys. Rev. B **84**, 073405 (2011).

[32] F. Molitor, S. Dröscher, J. Güttinger, A. Jacobsen, C. Stampfer, T. Ihn, and K. Ensslin, Appl. Phys. Lett. **94**, 222107 (2009).

[33] W. G. van der Viel, S. De Franceschi, J. M. Elzerman, T. Fujisawa, S. Tarucha, and L. P. Kouwenhoven, Rev. Mod. Phys. **75**, 1 (2003).

[34] P. Recher, J. Nilsson, G. Burkard, and B. Trauzettel, Phys. Rev. B **79**, 085407 (2009).

[35] F. Libisch, S. Rotter, J. Güttinger, C. Stampfer, and J. Burgdörfer, Phys. Rev. B **81**, 245411 (2010).

[36] J. A. Folk, C. M. Marcus, R. Berkovits, I. L. Kurland, I. L. Aleiner, and B. L. Altshuler, Phys. Scr. **T90**, 26 (2001).

[37] M. B. Lundeberg and J. A. Folk, Phys. Rev. Lett. **105**, 146804 (2010).

[38] M. B. Lundeberg and J. A. Folk, Nat. Phys. **5**, 894 (2009).

[39] S. S. Rao, A. Stesmans, K. Keunen, D. V. Kosynkin, A. Higginbotham, and J. M. Tour, Appl. Phys. Lett. **98**, 083116 (2011).

[40] N. Tombros, A. Veligura, J. Junesch, M. H. D. Guimaraes, I. J. Vera-Marun, H. T. Jonkman, and B. J. van Wees, Nature Phys. **7**, 697 (2011).

[41] M. Moreno-Moreno, A. Castellanos-Gomez, G. Rubio-Bollinger, J. Gomez-Herrero, and N. Agrait, Small **5**, 924 (2009).

[42] Z. Shi, R. Yang, L. Zhang, Y. Wang, D. Liu, D. Shi, E. Wang, and G. Zhang, Adv. Mater. **23**, 3061 (2011).